Inorg. Chem. **2004**, *43*, 7726–7734

Ligand Oxidations in High-Spin Nickel Thiolate Complexes and Zinc Analogues

Balwant S. Chohan,[†,‡] Steven C. Shoner,[§] Julie A. Kovacs,[§] and Michael J. Maroney*[,†]

Department of Chemistry, University of Massachusetts, Amherst, Massachusetts 01003, and Department of Chemistry, University of Washington, Seattle, Washington 98195

Received July 7, 2004

Oxidations of a trigonal-bipyramidal, high-spin Ni(II) dithiolate complex of a pentadentate, N_3S_2-donor ligand, N1,N9-bis(imino-2-mercaptopropane)-1,5,9-triazanonane) nickel(II), and the structurally analogous Zn(II) complex, lead to oxidations of the ligand. Oxidation of the Ni(II) complex with I_2 produces a novel Ni(II) macrocyclic cationic complex containing a monodentate disulfide ligand (**2**). Crystals of the I_3^- salt of the complex form in the triclinic space group P_1 with cell dimensions $a = 8.508(3)$ Å, $b = 9.681(2)$ Å, $c = 14.066(4)$ Å, angles $\alpha = 90.97(2)°$, $\beta = 91.61(3)°$, $\gamma = 90.83(2)°$, and $Z = 2$. The structure was refined to $R = 6.31\%$ and $R_w = 16.63\%$ ($I > 2\sigma(I)$). Oxidation of the Ni(II) complex with O_2 leads to the formation of a novel pentadentate bis-iminothiocarboxylate complex with trigonal-bipyramidal geometry (**3**). This neutral product crystallizes in the monoclinic space group $P2_1/c$ with cell dimensions $a = 13.625(3)$ Å, $b = 7.605(5)$ Å, $c = 14.902(4)$ Å, angles $\alpha = \gamma = 90°$, $\beta = 102.81(2)°$, and $Z = 4$. The structure was refined to $R = 7.18\%$ and $R_w = 17.86\%$ ($I > 2\sigma(I)$). Oxidation of the Zn(II) dithiolate analogue with O_2 leads to the formation of the Zn(II) complex of the pentadentate bis-iminothiocarboxylate ligand. The neutral complex is isomorphous with the Ni(II) complex and crystallizes in the monoclinic space group $P2_1/c$ with cell dimensions $a = 13.8465(4)$ Å, $b = 7.6453(2)$ Å, $c = 15.0165(6)$ Å, angles $\alpha = \gamma = 90°$, $\beta = 103.2140(11)°$, and $Z = 4$. The structure was refined to $R = 3.96\%$ and $R_w = 9.45\%$ ($I > 2\sigma(I)$). Details of the crystal structures are reported. Kinetics of the O_2 reactions show that the reactions of the Ni(II) and Zn(II) dithiolates follow the rate law, Rate $= k_2$[**1**][O_2], with $k_2 = 1.81$ M^{-1} s^{-1} for the Ni(II) complex and $k_2 = 1.93 \times 10^{-2}$ M^{-1} s^{-1} for the Zn(II) complex. The O_2 oxidation of the high-spin Ni(II) thiolate complex was found to follow a similar oxidation mechanism to those of low-spin Ni(II) complexes, which form transient persulfoxide intermediates that yield S-oxidation products. In the case of the high-spin system reported here, the transient persulfoxide intermediate gives rise to an alternative ligand oxidation product, a bis-iminothiocarboxylate complex, because of the reactivity of the ligand, which contains a methylene with acidic H atoms α to the thiolate sulfur. The proposed mechanism is supported by studies of the analogous Zn dithiolate complex, which gives rise to the analogous bis-iminothiocarboxylate product (**5**).

Introduction

Thiolate ligands in transition-metal complexes react with O_2 or H_2O_2 to form disulfides and sulfoxy compounds including sulfenates, sulfinates, and sulfonates.[1−17] These reactions are of significant biological importance. Cysteine oxygenates are intermediates and products of the catabolism of cysteine,[18] and altered sulfur oxidation chemistry is associated with a number of disease states.[19−25] Disulfides play impor-

* Author to whom correspondence should be addressed. Email: mmaroney@chemistry.umass.edu.

† University of Massachusetts.

‡ Current Address: Department of Chemistry and Biochemistry, Susquehanna University, Selinsgrove, PA 17870.

§ University of Washington.

(1) Mirza, S. A.; Pressler, M. A.; Kumar, M.; Day, R. O.; Maroney, M. J. *Inorg. Chem.* **1993**, *32*, 977.

(2) Kumar, M.; Colpas, G. J.; Day, R. O.; Maroney, M. J. *J. Am. Chem. Soc.* **1989**, *111*, 8323.

(3) Mirza, S. A.; Day, R. O.; Maroney M. J. *Inorg. Chem.* **1996**, *35*, 1992.

(4) Farmer, P. J.; Solouki, T.; Soma, T.; Russell, D. H.; Darensbourg, M. Y. *Inorg. Chem.* **1993**, *32*, 4171.

(5) Farmer, P. J.; Solouki, T.; Mills, D. K.; Soma, T.; Russell, D. H.; Reibenspies, J. H.; Darensbourg, M. Y. *J. Am. Chem. Soc.* **1992**, *114*, 4601.

(6) Mills, D. K.; Reibenspies, J. H.; Darensbourg, M. Y. *Inorg. Chem.* **1990**, *29*, 4364.

(7) Farmer, P. J.; Verpeaux, J. N.; Amatore, C.; Darensbourg, M. Y.; Musie, G. *J. Am. Chem. Soc.* **1994**, *116*, 9355.

10.1021/ic049110n CCC: $27.50
Published on Web 11/02/2004

tant structural and redox roles in proteins,[26−28] and oxidation of cysteine sulfur is also believed to tune the properties of metalloenzyme active sites, such as in iron-containing nitrile hydratases,[29−31] where cysteine is present in thiolate, sulfenate, and sulfinate redox states. Reactions involving sulfur oxidations have been extensively studied in low-spin, diamagnetic Ni(II) complexes.[1−17] Without exception, these reactions result in the oxidation of the sulfur centers. The reactions with O_2 are distinct from reactions with H_2O_2 in that the former can lead to products incorporating both atoms of O_2 (a four-electron, dioxygenase-like oxidation), whereas peroxide sequentially oxidizes S by two electrons with the transfer of one O atom. Here, we examine oxidations of a high-spin Ni(II) alkylthiolate complex (N1, N9-bis(imino-2-mercaptopropane)-1,5,9-triazanonane nickel(II) (**1**)) that also lead to ligand oxidation. As is the case in the low-spin systems, one-electron oxidations of thiolate ligands result in the formation of disulfides, in this case forming a novel macrocyclic complex (**2**). In contrast to the low-spin systems, the product of oxidation of (**1**) with O_2 is a novel bis-iminothiocarboxylate complex (**3**) that results from the oxidation of a carbon center in the ligand. Oxidation of the analogous Zn thiolate complex (**4**) yields the analogous bis-iminothiocarboxylate oxidation product (**5**), indicating that oxygen activation by the metal center is not involved.The iminothiocarboxylate complexes are stable compounds, but the nickel complex undergoes further oxidation under prolonged exposure to O_2. Here, we report synthetic details for the formation of the primary oxidation products and kinetic studies that support an oxidation mechanism similar to that suggested for low-spin Ni(II) complexes[1] but where the acidity of the C−H protons captures the presumed persulfoxide intermediate and alters the final oxidation product.

Chart 1. Structures of Reactants and Products

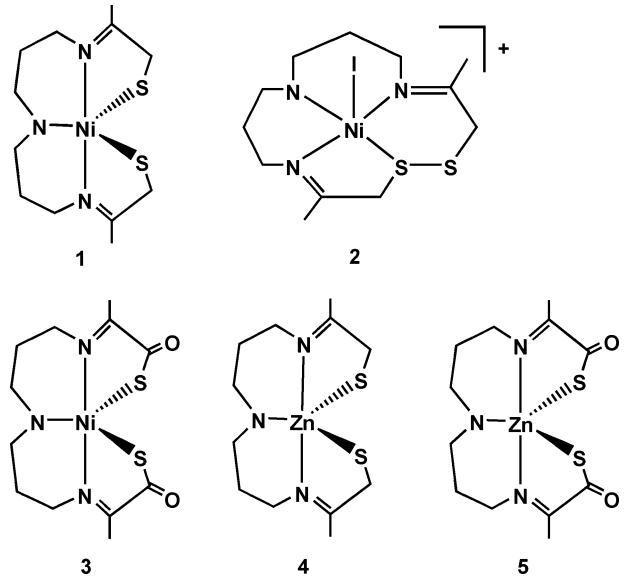

Experimental Section

Synthesis and Characterization. General Methods. The solvents used were dried by conventional methods[32] and stored under nitrogen or argon atmospheres. Except where noted, all starting materials were of reagent grade and used as received. The silica gel used for chromatographic separations was Aldrich grade 62, 60−200 mesh. Thin-layer chromatography (TLC) was used qualitatively to judge the number of components and to predict the general order of elution prior to separation by column chromatography. The TLC plates used were Whatman Flexback with fluorescent indicator, 60 Å size, 250 μm thickness. Except as noted, all synthetic procedures and manipulations were carried out under an argon atmosphere via use of Schlenk techniques. Samples for microanalysis were ground to a fine powder and vacuum desiccated over P_4O_{10} prior to analysis at the University of Massachusetts Microanalytical Laboratory.

N1,N9-Bis(imino-2-mercaptopropane)-1,5,9-triazanonane) Nickel(II), 1. This five-coordinate, high-spin Ni(II) dithiolate complex was prepared as previously described.[33] FAB-MS(+) *m*/*z* (relative intensity): 332.0 (100) (calcd for $NiC_{12}H_{24}N_3S_2^+$, 332.1); 300.0 (74) (calcd for $NiC_{12}H_{24}N_3S^+$, 300.1) (Supporting Information).

Iodo-(4,14-dimethyl-1,2-disulfido-5,9,13-triazacyclopentadeca-4,13-diene-S^1,N^5,N^9,N^{13}) Nickel(II) Triiodide, 2. Complex **1** (410 mg, 1.24 mmol) was dissolved in CH_2Cl_2 (80 mL) in a 250 mL

(8) Grapperhaus, C. A.; Darenbourg, M. Y. *Acc. Chem. Res.* **1998**, *31*, 451.
(9) Schrauzer, G. N.; Zhang, C.; Chadha, R. *Inorg. Chem.* **1990**, *29*, 4104.
(10) Henderson, R. K.; Bouwman, E.; Spek, A. L.; Reedijk, J. *Inorg. Chem.* **1997**, *36*, 4616.
(11) Maroney, M. J.; Choudhury, S. B.; Bryngelson, P. A.; Mirza, S. A.; Sherrod, M. J. *Inorg. Chem.* **1996**, *35*, 1073.
(12) Maroney, M. J.; Allan, C. B.; Chohan, B. S.; Choudhury, S. B.; Gu, Z. *Transition Metal Sulfur Chemistry, Biological and Industrial Significance*; Stiefel, E. I., Matsumoto, K., Eds.; ACS Symposium Series 653; American Chemical Society: Washington, DC, 1996.
(13) Grapperhaus, C. A.; Maguire, M. J.; Tuntulani, T.; Darensbourg, M. Y. *Inorg. Chem.* **1997**, *36*, 1860.
(14) Grapperhaus, C. A.; Darensbourg, M. Y.; Sumner, L. W.; Russell, D. H., *J. Am. Chem. Soc.* **1996**, *118*, 1791.
(15) Font, I.; Buonomo, R.; Reibenspies, J. H.; Darensbourg, M. Y., *Inorg. Chem.***1993**, *32*, 5897.
(16) Harrop, T. C.; Olmstead, M. M.; Mascharak, P. K. *Chem. Commun.* **2003**, 410.
(17) Kaasjager, V. E.; Bouwman, E.; Gorter, S.; Reedijk, J.; Grapperhaus, C. A.; Reibenspies, J. H.; Smee, J. J.; Darensbourg, M. Y.; Derecskei-Kovacs, A.; Thomson, L. M. *Inorg. Chem.*, **2002**, *41*, 1837.
(18) Allison, W. S. *Acc. Chem. Res.*, **1976**, *9*, 293.
(19) Pean, A.; Steventon, G. B.; Waring, R. H.; Foster, H.; Sturman, S.; Williams, A. C. *J Neurol. Sci.* **1994**, *124*, 59.
(20) Davies, M. H.; Ngong, J. M.; Pean, A.; Vickers, C. R.; Waring, R. H.; Elias, E. *J. Hepatol.* **1995**, *22*, 551.
(21) Emery, P.; Bradley, H.; Arthur, V.; Tunn, E.; Waring, R. *Br. J. Rheumatol.* **1992**, *31*, 449.
(22) Finkel, T. *FEBS Lett.* **2000**, *476*, 52.
(23) Claiborne, A.; Yeh, J. I.; Mallett, T. C.; Luba, J.; Crane, E. J.; Charrier, V.; Parsonage, D. *Biochemistry* **1999**, *38*, 15407.
(24) Perry, T. L.; Norman, M. G.; Yong, V. W.; Whiting, S.; Crichton, J. U.; Hansen, S.; Kish, S. J. *Ann. Neurol.* **1985**, *18*, 482.
(25) Hayflick, S. J.; Westaway, S. K.; Levinson, B.; Zhou, B.; Johnson, M. A.; Ching, K. H. L.; Gitschier, J. *N. Engl. J. Med.* **2003**, *348*, 33.
(26) Branden, C. I.; Tooze J. *Introduction to Protein Structure*, 2nd ed.; Garland Publishing: New York, 1999.
(27) Aslund, F.; Beckwith, J. *Cell* **1999**, *96*, 751.
(28) Aslund, F.; Zheng, M.; Beckwith, J.; Storz, G. *Proc. Natl. Acad. Sci. U.S.A.* **1999**, *96*, 6161.
(29) Tsujimura, M.; Dohmae, N.; Odaka, M.; Chijimatsu, M.; Takio, K.; Yohda, M.; Hocino, M.; Nagashima, S.; Endo, I. *J. Biol. Chem.* **1997**, *272*, 29454.
(30) Bonnet, D.; Stevens, J. M.; Alves de Sousa, R.; Sari, M.; Mansuy, D.; Artuad, I. *J. Biochem.* **2001**, *130*, 227.
(31) Murakami, Y.; Nojiri, M.; Nakayama, H.; Odaka, M.; Yohda, M.; Dohmae, N.; Takio, K.; Nagamune, T.; Endo, I. *Protein Sci.* **2000**, *9*, 1024.
(32) Riddick, J. A.; Bunger, W. B.; Sakano, T. K. *Organic Solvents*, 4th ed.; J. Wiley and Sons: New York, 1986.
(33) Shoner, S. C.; Olmstead, M. M.; Kovacs, J. A. *Inorg. Chem.* **1994**, *33*, 7.

round-bottomed flask. Iodine (627 mg, 2.47 mmol) was dissolved in CH_2Cl_2 (10 mL) and added dropwise to the solution of **1**, causing an immediate color change from green to yellow-green. The mixture was stirred overnight, whereupon it became dark green and produced a fine brown precipitate. The mixture was filtered, and the volume of the filtrate was reduced to 25 mL, and the solution was refiltered. Slow evaporation of the solvent, in air, over a period of 6 weeks yielded green-black crystals of **2** suitable for X-ray diffraction. In an identical experiment, the product was precipitated by addition of diethyl ether to the final filtered solution to yield a dark-green solid. The solid was filtered, washed with ether, and dried in vacuo. Yield = 861 mg (83%). Anal. Calcd for $NiC_{12}H_{23}N_3S_2I_4$: C, 17.17; H, 2.76; N, 5.01; I, 60.53. Found: C, 16.83; H, 2.62; N, 4.86; I, 58.6. (Note: Samples with such high iodine content often do not allow complete combustion[34]). μ_{eff} = 2.86μ_B (n = 2) as solid, 2.97μ_B in solution. IR (cm^{-1}): ν(C=N) 1640s, ν(C−N) 1060s, ν(Ni−I) 345w. ESI-MS(+) *m*/*z*, (relative intensity): 457.8 (61) (calcd for $NiC_{12}H_{23}N_3S_2I^+$, 458.0); 329.9 (100) (calcd for $NiC_{12}H_{22}N_3S_2^+$, 330.1) (Supporting Information).

N1,N9-Bis(imino-2-mercapto-2-keto-propane)-1,5,9-triazanonane Nickel(II), 3. Complex **1** (120 mg, 0.361 mmol) was dissolved in dimethylformamide (DMF) (40 mL) in a 100 mL round-bottomed flask fitted with a septum. Oxygen was bubbled into the solution via a needle for 42 min (three half-lives), causing a color change from grass green to orange-brown. To stop the reaction, nitrogen was bubbled through the solution for an additional 10 min. The solvent was removed by rotary evaporation under reduced pressure (but not elevated temperatures). The solid obtained was redissolved in a minimum amount of methanol and loaded onto a silica gel column (1.5 in. × 17 in.), which was prepared with dry methanol under nitrogen. Four fractions were eluted with methanol: (1) unreacted complex **1** (green), yield = 10.8 mg (9%) eluted first, followed by (2) a dark-green fraction corresponding to **2**, (3) a light brown fraction, and (4) a dark brown-black fraction. All of the eluted fractions were collected and stored under an argon atmosphere. Brown-black material that was insoluble in methanol, ethanol, or acetonitrile remained on top of the column and was not further investigated. The chromatographically separated fractions were concentrated, and the products were precipitated by addition of diethyl ether, filtered, washed with diethyl ether, and dried in vacuo. The second fraction produced a dark-green solid that constituted the major soluble oxidation product, **3** (41.6 mg, 32%), and was crystallized under strict anaerobic conditions from a mixture (4:1) of methanol and diethyl ether to give diffraction quality crystals after 12 days at room temperature. Anal. Calcd for $NiC_{12}H_{19}N_3S_2O_2$: C, 40.02; H, 5.32; N, 11.67. Found: C, 39.35; H, 5.46; N, 11.27. μ_{eff} = 2.92μ_B (n = 2). IR (cm^{-1}): 3210m 1640s, 1660s, 1600s, 1360m, 465m. UV−vis, λ (nm) (ϵ (M^{-1} cm^{-1})): 307 (1210), 399sh (790). ESI-MS(+) *m*/*z*, (relative intensity): 360.0 (100) (calcd for $NiC_{12}H_{20}N_3S_2O_2^+$, 360.0). Complex **3** is stable in air in the solid state for short periods of time but is deliquescent and reacts over extended periods of time (weeks) to give a brown-black insoluble product.

The remaining fractions were characterized by mass spectrometry (Supporting Information) and microanalysis. For fraction 3, ESI-MS(+) *m*/*z* (relative intensity): 260.1 (100) (calcd for $C_6H_{14}NS_2O_6^+$, 260.0), the mass spectrum lacks the features associated with natural abundance Ni isotopes, indicating demetalation has occurred in addition to ligand oxidation. For fraction 4, ESI-MS(+) *m*/*z* (relative intensity): 328.0 (100) (calcd for $NiC_9H_{22}N_2SO_5^+$,328.1). The empirical formulas determined by ESI-MS were used to calculate an elemental composition that is in reasonable agreement with the microanalytical results. For fraction 3, anal. calcd for $C_6H_{13}NS_2O_6$: C, 27.78; H, 5.06; N, 5.41; S, 24.69. Found: C, 27.75; H, 4.63; N, 5.15; S, 23.21. Anal. calcd for $NiC_9H_{21}N_2SO_5$ (fraction 4): C, 33.02; H, 6.47; N, 8.56; S, 9.77. Found: C, 32.90; H, 5.20; N, 9.29; S, 11.02. In both cases, the data show that the parent ligand backbone is not intact. For this reason, these products were not examined further.

N1,N9-Bis(imino-2-mercaptopropane)-1,5,9-triazanonane) Zinc(II), 4. This Zn(II) dithiolate complex is isostructural with **1** and was prepared as previously described.[35] The complex can be handled as a solid in air; however over long periods of time (>2 months), it becomes orange , presumably because of surface oxidation. For this reason, samples of **4** were stored in sealed vials or in an evacuated desiccator over P_4O_{10}. FAB-MS(+) *m*/*z* (relative intensity): 338.0 (100) (calcd for $ZnC_{12}H_{24}N_3S_2^+$, 338.1); 306.0 (36) (calcd for $ZnC_{12}H_{24}N_3S)^+$, 306.1) (Supporting Information).

N1,N9-Bis(imino-2-mercapto-2-keto-propane)-1,5,9-triazanonane) Zinc(II), 5. Complex **4** (145 mg, 0.428 mmol) was dissolved in DMF (75 mL) in a 100 mL round-bottomed flask that was fitted with a septum. Oxygen was bubbled into the solution via a needle for 70 h (four half-lives). During this time, the initially colorless solution became pale orange, and a small amount of a very fine white precipitate formed. The reaction was stopped by bubbling nitrogen through the solution for an additional 20 min, and the solution was filtered to remove the precipitate, which was insoluble in DMF, methanol, acetonitrile, and water. The solvent was then removed from the filtrate by rotary evaporation under reduced pressure (but not elevated temperatures). The yellow solid obtained was redissolved in a minimum volume of methanol and loaded onto a silica gel column (1.5 in. × 16 in.), which was prepared with dry methanol under nitrogen. Three fractions were eluted with methanol: (1) a colorless fraction identified as unreacted complex **4** (7.3 mg, 5% yield), (2) the major product, a green-orange fraction corresponding to **5** (72 mg, 46% yield), and (3) a small amount of a dark orange-brown fraction. The fractions were concentrated on a rotary evaporator, and the products were precipitated by addition of diethyl ether, filtered, washed with ether, and dried in vacuo. The second fraction was successfully crystallized by slow evaporation of a DMF solution in air over a period of 3 months to give diffraction quality crystals. Complex **5** is very stable in air. Anal. Calcd for $ZnC_{12}H_{19}N_3S_2O_2$: C, 39.29; H, 5.22; N, 11.46; Zn, 17.83. Found: C, 39.63; H, 5.70; N, 10.86; Zn, 17.17. The H and N microanalysis suggests the presence of a trace impurity in the bulk sample that cannot be accounted for by solvent. The crystal structure of **5** does not reveal the presence of solvent and establishes the elemental composition of the product as given above. IR (cm^{-1}): 3200m, 1650s, 1660s, 1590s, 1360m, 440m. UV−vis λ (nm) (ϵ ($M^{-1}cm^{-1}$)): 301 (890), 349 (730), 391 (650). ESI-MS(+) *m*/*z* (relative intensity): 366.0 (100) (calcd for $ZnC_{12}H_{20}N_3S_2O_2^+$, 366.0) (Supporting Information).

ESI-MS was used to determine an empirical formula for fraction 3. ESI-MS(+) *m*/*z* (relative intensity): 266.0(100) (calcd for $ZnC_8H_{14}N_2SO_2)^+$, 266.0). This formula was then used to calculate a theoretical microanalysis for fraction 3 that is reasonably consistent with the values found. Anal. Calcd for $ZnC_8H_{13}N_2SO_2$: C, 36.03; H, 4.91; N, 10.51; Zn, 24.52. Found: C, 35.08; H, 5.57; N, 10.35; Zn, 23.83. ESI-MS and microanalysis of fraction 3 indicate that the ligand backbone is not intact in this product, and so it was not examined further. (Supporting Information).

(34) Dabkowski, G. Personal Communication, 1999.

(35) Shoner, S. C.; Humphreys, K. J.; Barnhart, D.; Kovacs, J. *Inorg. Chem.* **1995**, *34*, 5933.

Physical Measurements. UV−vis spectra were obtained using Perkin-Elmer Lambda 3840, Hewlett-Packard 8453, or Olis 4300 Cary-14 instruments. UV−vis kinetic measurements were recorded using a flow cell (Starna Cells Inc., type 73-Q-10-T). For determination of kinetic data, reactions were run in a jacketed reaction vessel attached to a circulating bath held at constant temperature. The temperature of the UV−vis cell was maintained using a thermostated cell holder. The wavelength monitored during the kinetic investigations was chosen to maximize the absorbance change between starting materials/intermediates and products. Each reaction was allowed to run to completion before the data was analyzed. The method of initial rates was employed for the kinetic analysis in order to avoid complications from further oxidation products.[36,37] Kinetic experiments varying the oxygen concentration in DMF were run under pseudo-first-order conditions. Pseudo-first-order rate constants were determined by iterative fits of the data using Igor Pro software (Wavemetrics Inc., Oregon); the reaction time followed was according to the initial rate method.[36,37] The order of the reactions with respect to $[O_2]$ was determined by varying the partial pressure of O_2 in an O_2/N_2 gaseous mixture, using a Matheson 7351H gas mixing apparatus. The concentration of O_2 in DMF is dependent on the solubility of O_2 in DMF; the concentration values at 15° and 30° are known,[1,38] and values at other temperatures were calculated from a van't Hoff plot. Thermodynamic activation parameters were calculated from Eyring plots[36,37] using the equation, $k_2 = (k/h)e^{(\Delta S^{\ddagger}/R)}e^{(-\Delta H^{\ddagger}/RT)}$, where k is the Boltzmann constant, h is Planck's constant, R is the ideal gas constant, and k_2 is the second-order rate constant. Oxygen uptake measurements were made by manometric methods using an apparatus similar to that described in the literature.[1,39,40] The amount of oxygen absorbed by the complex in DMF solution was corrected for the amount of O_2 taken up by DMF over the same period of time, using uptake measurements made on the pure solvent.

Solid-state magnetic susceptibilities were obtained on Johnson Matthey (MK-1 and MSB-1) magnetic susceptibility balances. The Evans technique for measurement of solution magnetic moments by NMR was also employed.[41,42] Routine proton NMR spectra were obtained by using a Bruker AC200 MHz FT-NMR spectrometer. IR data for solid samples (as KBr disks) were obtained by using a Perkin-Elmer 783 IR spectrometer.

Electrospray ionization mass spectrometry (ESI-MS and MS/MS and $(MS)^n$) measurements were made at the University of Massachusetts Mass Spectrometry Center, using an Esquire LC/MS 32 instrument. Fast atom bombardment mass spectrometry (FAB-MS) measurements were made by Professor J. Leary (University of California, Berkeley) on a VG70 instrument, using a glycerol matrix. The reported m/z values in the synthetic section correspond to the most intense peak in an isotopic cluster, and the calculated/theoretical m/z values are based on the masses of the most common isotopes (monoisotopic mass). Determinations of molecular formulas were also based on simulation of peaks in an isotopic cluster assuming the natural abundance of stable isotopes.

(36) Wilkins, R. G. *Kinetics and Mechanisms of Reactions of Transition Metal Complexes*, 2nd ed.; Weinheim VCH Publishers: New York, 1991.
(37) Laidler, K. J. *Chemical Kinetics*, 3rd ed.; Harper and Row Publishers: New York, 1987.
(38) Mirza, S. A. Ph.D. Dissertation, Bhavnagar University, India, 1989.
(39) Umbreit, W. W.; Burris, R. H.; Stauffer, J. F. *Manometric Techniques*; Burgess Publishing: Minneapolis, 1957.
(40) Chen, D.; Martell, A. E. *Inorg. Chem.* **1987**, *26*, 1026.
(41) Evans, D. F. *J. Chem. Soc.* **1959**, 2003.
(42) Grant, D. L. *J. Chem. Educ.* **1995**, *72*, 39.

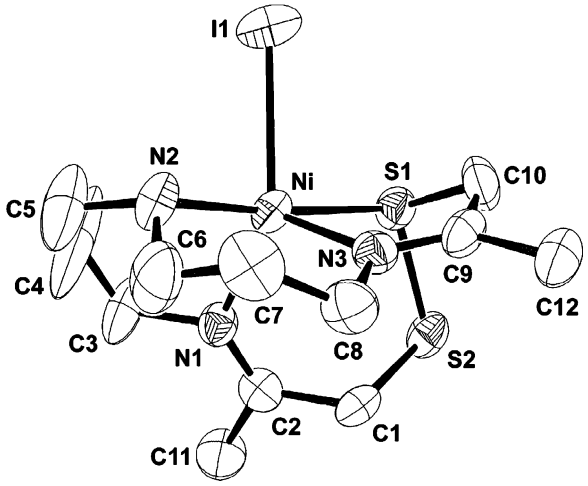

Figure 1. ORTEP plot of **2** in [**2**]I_3 with thermal ellipsoids at 50% probability. Hydrogen atoms have been omitted for clarity.

Single-crystal X-ray crystallographic diffraction studies were performed by Dr. A. Chandrasekaran and Professor R. Day at the University of Massachusetts, using an Enraf Nonius CAD4 diffractometer and a Nonius Kappa CCD diffractometer, and graphite monochromated Mo Kα radiation ($\lambda = 0.71073$ Å). Specific details for all of the complexes that were crystallographically studied can be found in the Supporting Information. The structures were solved by direct methods and difference Fourier techniques and were refined by the full-matrix least-squares methods. Refinements were based on F^2, and computations were performed using SHELXL-97 for solution and refinement.[43] The plotting program ORTEP-3 for Windows was used for the structural diagrams.[44]

Results and Discussion

Oxidation of 1 with I_2: Synthesis, Characterization, and Structure of 2. Oxidation of **1** with I_2 gives a high yield of a disulfide complex, **2** (eq 1), that results from the one-electron oxidation and intramolecular coupling of both thiolate ligands present in the starting material. Magnetic susceptibility measurements of **2** ($\mu_{eff} = 2.86\mu_B$, solid; $2.97\mu_B$, solution) are indicative of a high-spin ($S = 1$) Ni(II) center in both the solid state and solution. The ESI-MS spectrum of **2** reveals an isotopic cluster of peaks for the parent cation at $m/z = 457.8$, which can be simulated well assuming naturally occurring isotopic abundances. Another peak, observed at $m/z = 329.9$, corresponds to the loss of HI from the parent complex (Supporting Information).

$$\mathbf{1} + 2I_2 \rightarrow \mathbf{2} \qquad (1)$$

The structure of **2** is shown in Figure 1 and pertinent bond lengths and angles are given in Table 1. The structure reveals that **2** crystallizes as discrete cations with triodide, I_3^-, as the counterion. The production of the intramolecular disulfide results in the formation of a novel tetradentate macrocyclic ligand, which is bound to nickel by three N atoms and one of the disulfide S atoms. A fifth ligand is provided by an iodide anion. The geometry of the nickel center is best

(43) Sheldrick, G. M. *Acta Crystallogr.* **1990**, *A46*, 467.
(44) Farrugia, L. J. *J. Appl. Crystallogr.* **1997**, *30*, 565.

Table 1. Selected Bond Lengths (Å) and Bond Angles (deg) for Complex **2**

Bond Lengths		Bond Angles	
Ni−S1	2.423(3)	S1−Ni−N1	91.5(3)
Ni−N1	2.049(9)	S1−Ni−N2	175.0(3)
Ni−N2	2.028(10)	S1−Ni−N3	84.1(3)
Ni−N3	2.019(10)	N1−Ni−N2	92.5(4)
Ni−I1	2.6753(18)	N1−Ni−N3	110.2(4)
S1−S2	2.048(4)	N1−Ni−I1	137.2(3)
		N2−Ni−I1	90.4(3)
		N3−Ni−I1	111.7(3)
		S1−Ni−I1	84.57(9)
		C1−S2−S1	102.6(3)
		S2−S1−Ni	109.07(15)
		C10−S1−Ni	89.5(4)
		C10−S1−S2	101.7(5)

described as distorted trigonal-bipyramidal ($\tau = 0.63$, where a value of 1 corresponds to ideal trigonal-bipyramidal geometry and 0 corresponds to ideal square pyramidal geometry)[45] with S1 and N2 occupying the axial positions. The S1−Ni−N2 angle is close to the ideal 180° (175.0(3)°); however the Ni1−Ni−N3 and the N−Ni−I angles deviate considerably from 120° because of the constraints imposed by the macrocyclic ligand. The S−S distance (2.048(4) Å) is typical of other disulfide S−S distances known in chelating N/S-donor ligands,[46−54] and the Ni−N, Ni−S, and Ni−I distances are appropriate for the high-spin formulation and are similar to those reported for the only other known five-coordinate Ni(II) disulfide complex.[46]

Oxidation of 1 with O_2: Synthesis, Characterization, and Structure of 3. Oxidation of **1** with O_2 in DMF gives a mixture of products, three of which can be separated on a silica gel column. The initial oxidation product is complex **3** (eq 2). The reaction was followed spectrophotometrically and exhibits isosbestic points at 435 and 582 nm that are maintained for about 52 min (ca. four half-lives) (Figure 2).

$$\mathbf{1} + 2O_2 \rightarrow \mathbf{3} \qquad (2)$$

The two limiting spectra involved are identical to those of pure samples of **1** (dotted line) and **3** (dashed line), indicating that **1** is converted to **3** according to eq 2 with no observable intermediates. Eventually, the isosbestic points are lost (spectra not shown), because of oxidation of **3** (see below). Further oxidation of **3** accounts for the fact that exhaustive oxidation of **1** consumes a total of 2.5 equiv of O_2 (Figure 3) rather than the 2 equiv required for formation of **3**.

Magnetic susceptibility measurements ($\mu_{eff} = 2.92\mu_B$, solid) are indicative of a high-spin ($S = 1$) Ni(II) center in

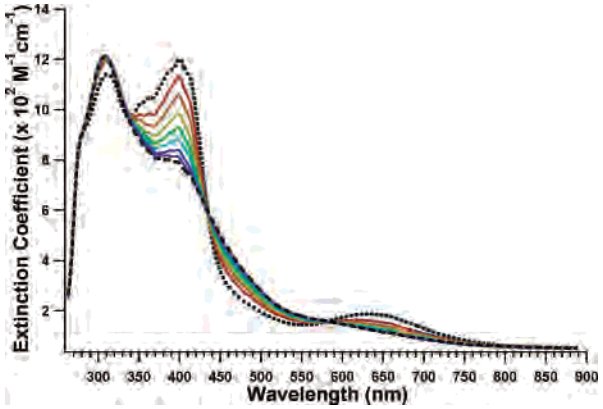

Figure 2. UV−vis spectral changes during the oxidation of **1** with O_2 in DMF. The spectrum of **1** in the absence of O_2 is shown as a dotted line. The dashed line represents the spectrum of isolated product, **3**. Spectra shown during the oxidation reaction at 25 °C (solid lines) were taken at time intervals t = 9, 11, 14, 16, 18, 33, 48, and 56 min.

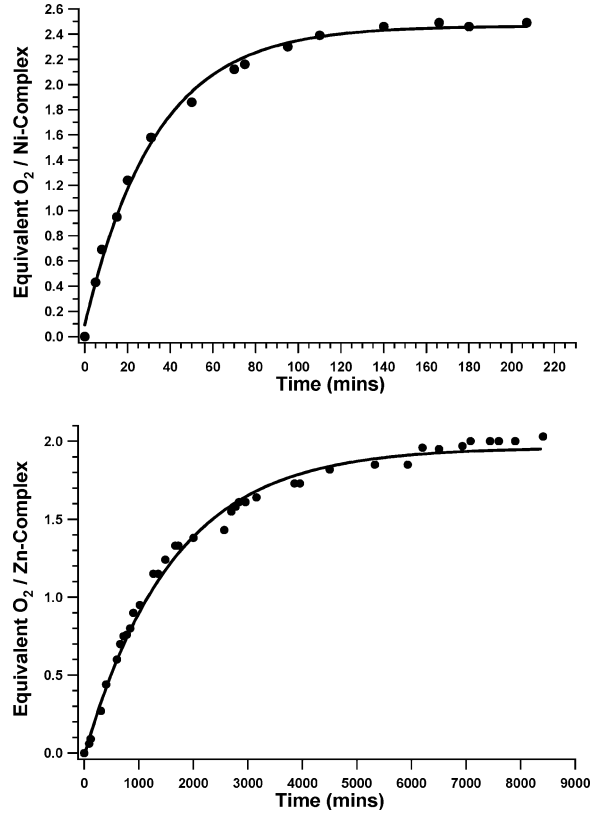

Figure 3. Manometric O_2 uptake measurements of complex **1** (top) and complex **4** (bottom).

3. The ESI-MS spectrum of **3** reveals an isotopic cluster of peaks that corresponds to a parent cation with $m/z = 360.0$ and is consistent with the addition of two O atoms to **1** (Figure 4).

The structure of **3** shows that the oxidation product is a novel bis-iminothiocarboxylate complex. There are very few structures that contain the β-iminothiocarboxylate moiety, and none of these are transition-metal complexes.[55−57] The structure of **3** is shown in Figure 5 and summarized in Table 2.

(45) Addison, W. A.; Rao, T. N,; Reedijk, J.; Rijn, J.; Verschoor, G. C. *J. Chem. Soc., Dalton Trans.* **1984**, 1349.
(46) Kumar, M.; Day, R. O.; Colpas, G. J.; Maroney, M. J. *J. Am. Chem. Soc.* **1989**, *111*, 5974.
(47) Warner, L. G.; Kadooka, M. M.; Seff, K. *Inorg. Chem.* **1975**, *14*, 1773.
(48) Riley, P. E.; Seff, K. *Inorg. Chem.* **1972**, *11*, 2993.
(49) Warner, L. G.; Ottersen, T.; Seff, K. *Inorg. Chem.* **1974**, *13*, 2529.
(50) Muller, A.; Krickemeyer, E.; Bogge, H.; Clegg, W.; Sheldrick, G. M. *Angew. Chem., Intl. Ed. Engl.* **1983**, *22*, 1006.
(51) Coucouvanis, D.; Patil, P. R.; Kanatzidis, M. G.; Detering, B.; Baenziger, N. G. *Inorg. Chem.* **1985**, *24*, 24.
(52) Weiss, J. *Z. Anorg. Allg. Chem.* **1985**, *521*, 44.
(53) Bonamico, M.; Dessy, G.; Fares, V.; Scaramuzza, L. *J. Chem. Soc. A* **1971**, 3191.
(54) Coxall R. A.; Harris S. G.; Henderson D. K.; Parsons S.; Tasker P. A.; Winpenny R. E. P.; *J. Chem. Soc., Dalton Trans.* **2000**, 2349.

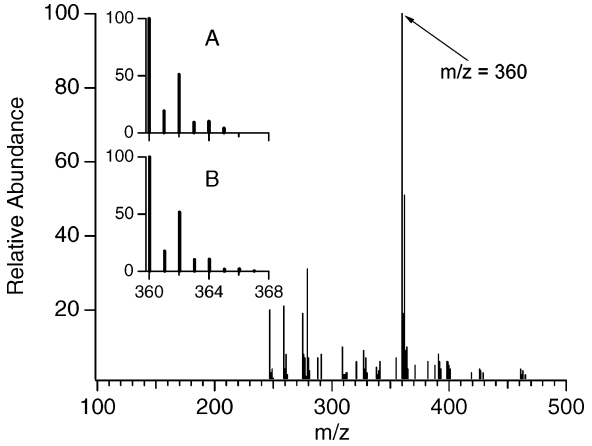

Figure 4. ESI-MS spectrum of **3** (top), expansion of ESI-MS peak at *m*/*z* = 360.0 (middle), and the simulated fit for the cation $(NiC_{12}H_{20}N_3S_2O_2)^+$ based on isotopic abundance (bottom).

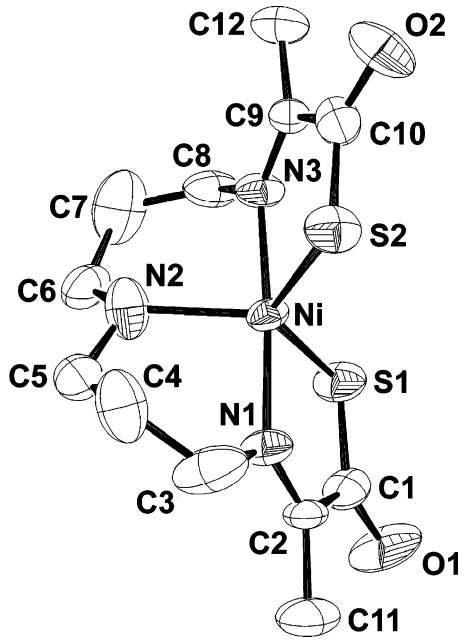

Figure 5. ORTEP plot of **3** with thermal ellipsoids at 50% probability. Hydrogen atoms have been omitted for clarity.

In contrast to the oxidation products observed for low-spin Ni(II) thiolates, oxidation occurs at the α-C atom rather than at the thiolate S atom. The neutral complex, **3**, features a pentacoordinate, distorted trigonal-bipyramidal Ni(II) center ($\tau = 0.78$)[45] that is structurally very similar to the starting complex, **1** ($\tau = 0.78$);[45] the largest structural changes are the oxidation of the C atoms to carbonyls and a reduction in the S−Ni−S angle from 135.3° to 129.1°.

Oxidation of 4 with O_2: Synthesis, Characterization, and Structure of 5. To address the role of metal-centered O_2 activation, we also examined the oxidation of the zinc complex. The zinc complex, **4**, is a structural analogue of **1**.[35] As was the case for the nickel complex (**1**), oxygenation of solutions of **4** in DMF produced a mixture of oxidation products, two of which were separated by chromatography on a silica gel column. The major product, and the primary oxidation product, is **5**, the zinc analogue of **3.** Exhaustive oxidation of **4** (Figure 3) shows that two O_2 molecules are involved in the conversion, consistent with eq 3.

$$\mathbf{4} + 2O_2 \rightarrow \mathbf{5} \qquad (3)$$

The structure of **5** is shown in Figure 6, summarized in Table 2, and features a bis-iminothiocarboxylate, similar to the corresponding nickel complex (**3**). The Zn center in **5** has distorted trigonal-bipyramidal geometry ($\tau = 0.80$)[45] and is very similar to the geometry found in the dithiolate, **4** ($\tau = 0.80$).[45] Other than the oxidation of α-C atoms to carbonyls, the structural changes involved in the conversion of **4** to **5** are even smaller than those involved in the conversion of **1** to **3.**

Table 2. A Comparison of Selected Bond Lengths (Å) and Bond Angles (deg) for Complexes **1**,[33] **3**, **4**,[35] and **5**

	1	**3**	**4**	**5**
		Bond Lengths		
M−S1	2.306(2)	2.317(2)	2.337(1)	2.3459(11)
M−S2	2.359(2)	2.324(3)	2.329(1)	2.3476(11)
M−N1	2.065(4)	2.040(7)	2.167(3)	2.139(3)
M−N2	2.068(4)	2.036(8)	2.142(4)	2.117(3)
M−N3	2.048(4)	2.031(7)	2.179(3)	2.151(3)
C1−O1		1.230(11)		1.263(5)
C10−O2	1.223(11)		1.265(5)	
		Bond Angles		
S1-M−S2	135.3(1)	129.10(11)	124.1(1)	122.18(4)
S1-M−N1	84.7(1)	84.2(2)		
S1-M−N2	123.7(2)	121.6(3)		
S2-M−N1	99.1(1)	99.5(2)		
S2-M−N2	101.0(1)	109.2(3)	117.2(1)	123.45(9)
S2-M−N3	83.6(1)	83.9(2)		
N1-M−N2	92.7(1)	90.8(3)		
N1-M−N3	177.3(2)	175.7(3)	170.0(1)	171.46(12)
S1−C1−O1		123.2(8)		124.1(3)
S1−C1−C2		118.6(6)		119.4(3)
S2−C10−O2		123.2(8)		122.8(4)
S2−C10−C9		118.2(7)		119.7(3)

Kinetics and Mechanism. The oxidation of **1** (eq 2) obeys a second-order rate law that is first-order in both the concentrations of complex and O_2, $d[\mathbf{3}]/dt = k_2[\mathbf{1}][O_2]$, where $k_2 = 1.81\ M^{-1}\ s^{-1}$. The reaction was monitored spectrophotometrically at 400 nm, and the resulting kinetic data are shown in Table 3. Sample kinetic data and an exponential fit are shown in Figure 7.

The dependence on $[O_2]$ was determined by measuring pseudo-first-order rate constants (k_{obs}) at 25 °C under different constant oxygen concentrations. The variation of the rate with $[O_2]$ is also shown in Figure 7.

The reaction rates were insensitive to the presence of the radical scavenger, 2,4,6-tri-*tert*-butyl phenol (10-fold excess), or the singlet oxygen scavenger, 1,4-diazabicyclo[2.2.2]-octane (10-fold excess). The second-order rate constant for the reaction was calculated from the observed first-order rate constant and the solubility of O_2 in DMF ($k_2 = k_{obs}/[O_2]$) (Experimental Section).

The activation parameters, $\Delta H^{\ddagger}$ and $\Delta S^{\ddagger}$,for the reaction of **1** with O_2 were calculated from the temperature dependence of k_2 and found to be 11.6 kcal/mol and −18.6 cal/K, respectively (Supporting Information).

(55) Al-Awadhi, H.; Al-Omran, F.; Elnagdi, M. H.; Infantes, L.; Foces-Foces, C.; Jagerovic, N.; Elguero, J. *Tetrahedron*, **1995**, *51*, 12745.
(56) Wipf, P.; Heimgartner, H. *Tetrahedron Lett.* **1984**, *25*, 5127.
(57) Wipf, P.; Brieri, J. H.; Heimgartner, H.; Nastopoulos, V.; Germain G. *Helv. Chim. Acta* **1987**, *70*, 1380.

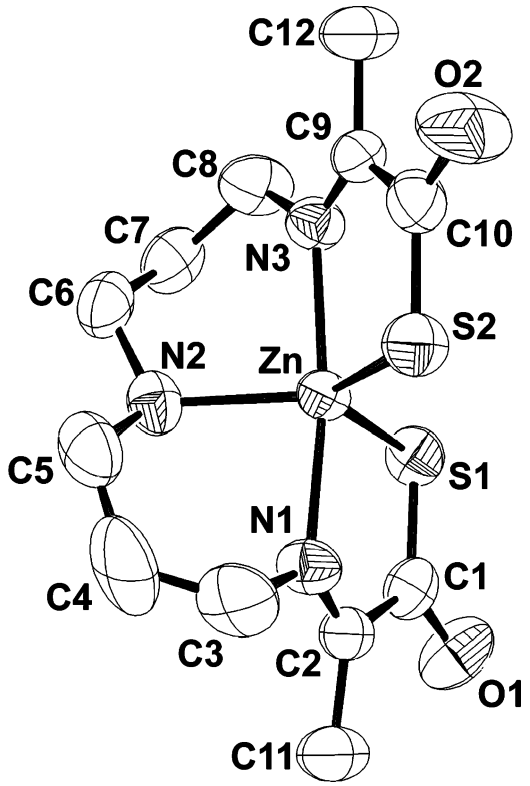

Figure 6. ORTEP plot of **5** with thermal ellipsoids at 50% probability. Hydrogen atoms have been omitted for clarity.

Table 3. Kinetic Data for the Oxygenation of Complex **1** and **4** in DMF

pO_2	temp (°C)	$k_{obs} \times 10^{-3}$ [a]	k_2 (M^{-1} s^{-1})
		Complex **1**	
0.20	25	1.54(2)	1.47
0.40	25	3.20(3)	1.53
0.50	25	4.35(1)	1.65
0.80	25	7.16(2)	1.72
1.0	25	9.45(3)	1.82
1.0	−15	0.45(6)	0.07
1.0	−5	0.97(5)	0.17
1.0	5	1.14(2)	0.21
1.0	15	3.95(6)	0.73
1.0	35	15.4(3)	3.06
1.0	41	21.9(4)	4.42
		Complex **4**	
0.20	25	1.42(4)	13.6
0.40	25	2.47(2)	11.8
0.50	25	4.00(2)	15.2
0.80	25	6.34(3)	15.2
1.0	25	10.0(3)	19.3
1.0	15	5.14(6)	9.54
1.0	30	13.8(5)	27.0
1.0	35	25.5(5)	50.5
1.0	41	43.7(6)	88.4

[a] Reported in s^{-1} for complex **1** and in M^{-1} s^{-1} for complex **4**.

The oxidation of **4** (eq 3) obeys the same rate law as the oxidation of **1** with $k_2 = 1.93 \times 10^{-2}$ M^{-1} s^{-1}. The kinetics of the oxidation of **4** to **5** (the zinc analogues of **1** and **3**) were examined following the same procedure employed for the oxidation of **1**, only monitoring the absorbance changes at 390 nm (Supporting Information). In this case, the spectra do not exhibit isosbestic points, but manometric O_2 uptake clearly establishes the stoichiometry of the reaction (eq 3) and indicates that only **5** was formed to an appreciable extent.

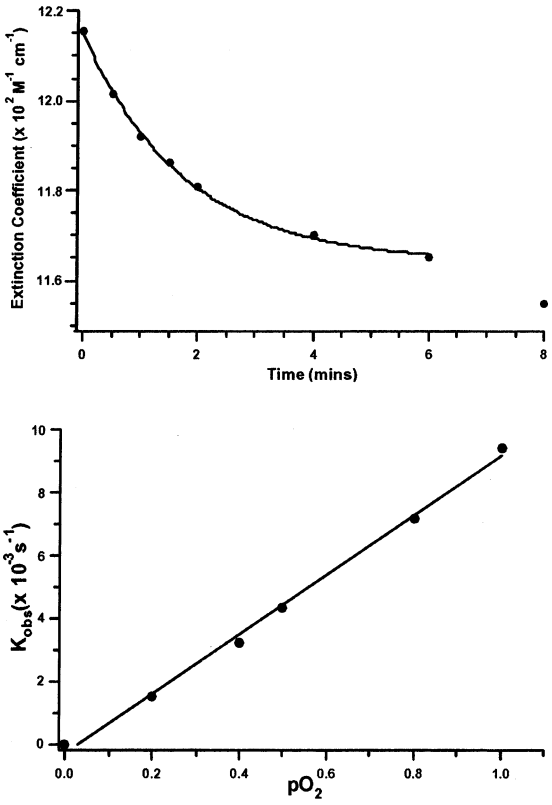

Figure 7. Kinetic data and fits for the oxidation of **1** with O_2. Depicted are changes in A_{400} with time (top) and oxygen dependence of the reaction rate at 25° C (bottom).

The activation parameters $\Delta H^{\ddagger}$ and $\Delta S^{\ddagger}$ for the reaction of **4** with O_2 to form **5** were found to be 14.8 kcal/mol and −16.2 cal/K, respectively (Supporting Information).

A hypothetical mechanism for the oxidation of **1** by O_2 is shown in Scheme 1. The fact that the oxidation is first order in $[O_2]$ and no intermediate is observed is consistent with a mechanism where the reaction of the first O_2 molecule is rate-determining and the subsequent O_2 reaction is fast. The values of $\Delta H^{\ddagger}$ and $\Delta S^{\ddagger}$ determined for the oxidation of **1** are similar to those observed for the low-spin Ni(II) complexes previously examined ($\Delta H^{\ddagger} = 13.1-14.7$ kcal/mol, $\Delta S^{\ddagger} = -18.7$ to -24.2 cal/mol),[1] indicating a similar transition state is involved in the oxidation of both high-spin and low-spin Ni(II) complexes. The small positive enthalpy and negative entropy values are typical of associative reaction mechanisms.[1,36,37,40] This is consistent with nucleophilic attack of the thiolate S atom on O_2, followed by O−O bond cleavage, as proposed for the reactions of the low-spin Ni(II) complexes.[1] The oxidation of the high-spin complex differs from that observed for low-spin complexes, where O−O bond scission produces an S-bound sulfinate ligand, because of the presence of a methylene C atom that is α to the S center and β with respect to an imine moiety. As such, the H atoms of the methylene C are acidic and can capture the open form of the persulfoxide intermediate (as opposed to the thiadioxirane form that appears to be involved in producing sulfinate ligands in the low-spin systems[1]). Proton abstraction by the persulfoxide, followed by O−O bond cleavage, produces a transient mono-oxygen-

Scheme 1. Proposed Mechanism for the Oxidation of **1** to **3**

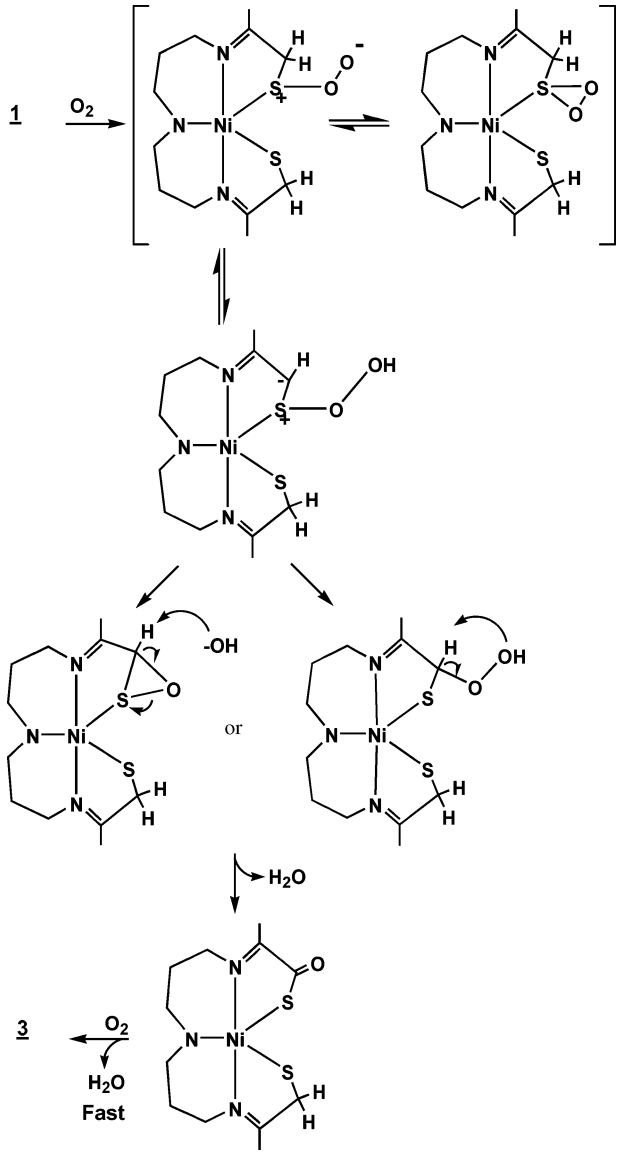

ated complex, which undergoes a second identical reaction at the remaining thiolate ligand to produce **3**. In contrast to the reactions of the low-spin Ni(II) thiolates, where the second thiolate S atom is rendered less nucleophilic by the formation of a sulfinate,[11,12,58] a faster rate is required for the second oxidation in the high-spin complex. Some insight into this can be gained by comparing the kinetics of high- and low-spin Ni(II) systems with that of the Zn complex, **4**.

Because the Zn analogue (**4**) has similar values of $\Delta H^{\ddagger}$ and $\Delta S^{\ddagger}$, and forms an analogous product, a similar mechanism would be expected. The fact that both the Ni complex and the Zn complex react in an identical fashion indicates that reductive activation of O_2 at the metal center leading to the formation of a peroxo intermediate and Ni(IV) does not play a role in the oxidation of **1**.

The high-spin Ni(II) complex (**1**) is about 2 orders of magnitude more reactive than the low-spin Ni(II) thiolate complexes previously examined ($k_{obs} \approx 1 \times 10^{-4}$ s^{-1}, and values of $k_2 \approx 2 \times 10^{-2}$ M^{-1} s^{-1} at 30°).[1] It is unclear why the high-spin Ni(II) complex is more reactive, but possible reasons include (1) more efficient reaction of the persulfoxide intermediate, (2) the spin-allowed nature of the reaction (both reactants in the high-spin case are $S = 1$, as is the product), or (3) the thiolates are more nucleophilic in the high-spin system, possibly because of dissociation of the thiolate prior to formation of the persulfoxide, leading to a higher concentration of transient persulfoxide in the initial equilibrium. The fact that the Zn complex, which would be expected to have more labile thiolate ligands, is 2 orders of magnitude less reactive than the Ni complex argues against thiolate dissociation prior to reaction with O_2. Calculations in progress[59] suggest that the Zn thiolates in **4** are slightly more nucleophilic than the Ni thiolates in **1**, as would be expected for the less covalent d^{10} ion, so the rates do not appear to correlate with S nucleophilicity. Rather, they appear to correlate with the spin-allowed nature of the reactions, since **4** ($S = 0$) reacts at a comparable rate to that observed for low-spin ($S = 0$) Ni(II) dithiolate complexes.[1]

Another question regarding the oxidation mechanism is why the second oxidation is faster than the first for both **1** and **4**, particularly because the oxidation of low-spin Ni(II) dithiolates reduces the reactivity of the remaining thiolate.[1] Oxidation of the dithiolates to monothiocarboxylates would be expected to decrease the nucleophilicity of the remaining thiolate via inductive effects. However, in **1** and **4**, the inductive effect should also increase the acidity of the C−H bond α to the remaining thiolate. It is possible that the increased acidity of the C−H bond dominates over the loss of S nucleophilicity. It is hoped that the calculations in progress will shed light on these points.

Conclusions

The oxidations of high-spin Ni(II) thiolate complexes were found to follow similar oxidation mechanisms to those of low-spin Ni(II) complexes. Reaction of **1** with I_2 leads to the formation of a novel macrocyclic product (**2**), featuring a monodentate disulfide S-donor, as was the case for a previously studied low-spin system.[46] This product is presumed to arise from the intramolecular coupling of transient thiyl radical-like species formed in the reaction. Reaction of **1** with O_2 appears to proceed via the same mechanism as the oxidation of low-spin thiolates, which form transient persulfoxide intermediates that yield S-oxidation products.[1] In the case of **1**, the transient persulfoxide intermediate gives rise to an alternative ligand oxidation product, a bis-iminothiocarboxylate complex, *because of the reactivity of the ligand*. This mechanism is supported by studies of the analogous Zn thiolate complex (**4**), which gives rise to the analogous bis-iminothiocarboxylate product (**5**). The stoichiometry of the reactions ($2O_2$/1Ni or $2O_2$/1Zn) points to the "peroxide-like" (or open form) reactivity of the persulfoxide intermediate in these cases.

(58) Weiss, M. C.; Goedken, V. L. *J. Am. Chem. Soc.* **1976**, *98*, 3389.

(59) Bryngelson, P. A.; Maroney, M. J. Unpublished work.

Acknowledgment. This work was supported in part by a grant from the NIH, GM-38829 (M.J.M.). Acknowledgment is also made to the donors of the Petroleum Research Fund, administered by the American Chemical Society, for partial support of this research. We thank Professor Julie Leary for FAB-MS data and Dr. A. Chandrasekaran and Dr. R. Day for crystallographic results. The University of Massachusetts X-ray Structural Characterization Laboratory is supported by a grant from the National Science Foundation (CHE-9974648).

Supporting Information Available: Tables of crystallographic data, atomic coordinates, bond lengths and angles, anisotropic displacement parameters, hydrogen coordinates, and X-ray crystallographic data in CIF format for compounds **2**, **3**, and **5**. Figures summarizing FAB-MS data for compounds **1** and **4**. Figures summarizing ESI-MS data for **2** and oxidation products of **1**, **5**, and **4**. Eyring plots for the oxygenation reactions of compounds **1** and **4**. UV−vis spectral data for the oxidation of **4**. This information is available free of charge via the Internet at http://pubs.acs.org.

IC049110N